

Supplementary Information for:

High performance acidic water electrooxidation catalysed by manganese-antimony oxides promoted by secondary metals

Sibimol Luke^{a,b,c,†}, Manjunath Chatti^{d,†}, Darcy Simondson^{d,†}, Khang N. Dinh^d, Brittany V. Kerr^e, Tam D. Nguyen^d, Gamze Yilmaz,^d Bernt Johannessen^f, Douglas R. MacFarlane^d, Aswani Yella^{b*}, Rosalie K. Hocking^{e*}, and Alexandr N. Simonov^{d*}

^a IITB-Monash Research Academy, IIT Bombay, Mumbai 400076, India

^b Department of Metallurgical Engineering and Materials Science, Indian Institute of Technology Bombay, Powai, Mumbai 400076, India

^c Department of Chemical Engineering, Monash University, Victoria 3800, Australia.

^d School of Chemistry, Monash University, Clayton, Victoria 3800, Australia

^e Department of Chemistry and Biotechnology, Swinburne University of Technology, Hawthorn, Victoria 3122, Australia

^f Australian Synchrotron, Clayton 3168, Victoria, Australia

* Corresponding authors:

aswani.yella@iitb.ac.in; rhocking@swin.edu.au; alexandr.simonov@monash.edu

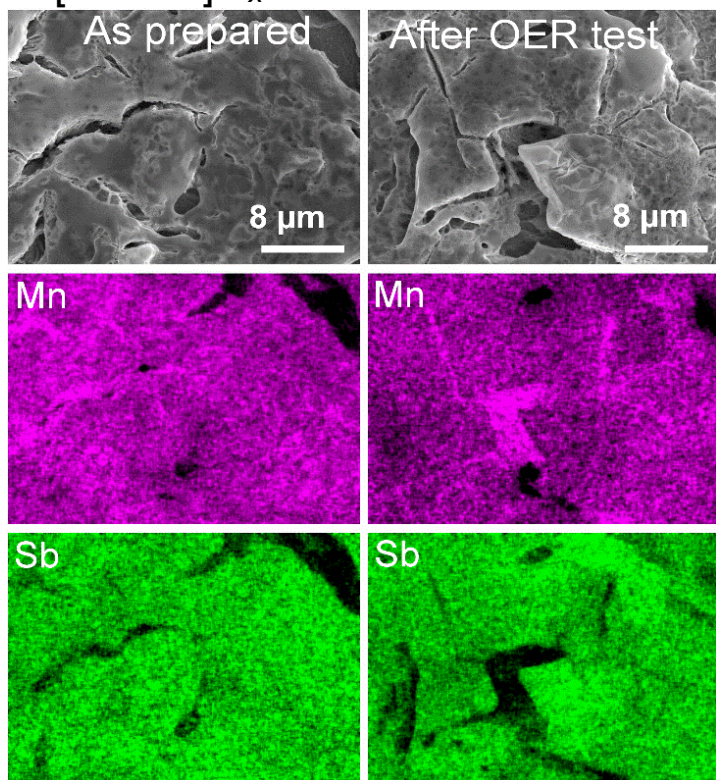
[†] *These authors contributed equally to this work*

TABLE OF CONTENTS

1 ENERGY DISPERSIVE X-RAY MAPPING	1
Figure S1. SEM-EDS mapping of [Mn+Sb]O _x and [MnPb + Sb]O _x before and after OER tests.....	1
2 X-RAY PHOTOELECTRON SPECTROSCOPY	2
Figure S2. High resolution Sb 3d + O 1s and C 1s (+ Ru 3d) spectra.....	2
Figure S3. High resolution Mn 2p spectra.....	3
Figure S4. High resolution Pb 4f spectra	4
Figure S5. High resolution Co 2p spectra	5
Figure S6. High resolution Cr 2p spectra	6
3 CHANGES IN THE COMPOSITION OF CATALYSTS DURING THE OER	7
Table S1. Relative concentration of metals on the catalysts surface before and after OER tests.....	7
Table S2. Corrosion of catalysts (%) during the OER in 0.5 M H ₂ SO ₄	7
4 EX SITU X-RAY ABSORPTION SPECTROSCOPY	8
Figure S7. XANES, EXAFS and FT-EXAFS data collected at the Sb K-edge	8
Figure S8. XANES, EXAFS and FT-EXAFS data collected at the Co K-edge	9
Figure S9. XANES, EXAFS and FT-EXAFS collected at the Pb L ₃ -edge.....	10
5 OER PERFORMANCE AND REPRODUCIBILITY AT 24 ± 2 °C	11
Figure S10. Potentiodynamic and galvanostatic data for [MnRu+Sb]O _x	11
Figure S11. Potentiodynamic and galvanostatic data for [MnCo+Sb]O _x	12
Figure S12. Potentiodynamic and galvanostatic data for [MnPb+Sb]O _x	13
Figure S13. Potentiodynamic and galvanostatic data for [MnCoPb+Sb]O _x	14
Figure S14. Potentiodynamic and galvanostatic data for [MnCr+Sb]O _x	15
6 CYCLIC VOLTAMMETRY AT 24 ± 2 °C	16
Figure S15. Full range cyclic voltammograms before and after the OER tests	16
Figure S16. Pre-catalytic regions of cyclic voltammograms before and after the OER tests	17
7 OER ACTIVITY OF THE CR- AND PB-BASED OXIDES	18
Figure S17. Potentiodynamic and galvanostatic data for Cr- and Pb-based catalysts.....	18
8 PERFORMANCE OF [MnCo+Sb]O_x WITH DIFFERENT MN : CO RATIOS	19
Figure S18. Effect of the Mn : Co initial ratio on the performance of the [MnCo+Sb]O _x catalysts.....	19
9 OER PERFORMANCE AND REPRODUCIBILITY AT 60 ± 1 °C	20
Figure S19. Chronopotentiogram for [MnCr+Sb]O _x	20
Figure S20. Potentiodynamic and galvanostatic data for [MnPb+Sb]O _x	20
Figure S21. Potentiodynamic and galvanostatic data for [MnCo+Sb]O _x	21
10 CYCLIC VOLTAMMETRY AT 60 ± 1 °C	22
Figure S22. Full range cyclic voltammograms before and after the OER tests	22
11 EXTENDED CHARACTERISATION OF POWDER CATALYSTS	23
Figure S23. TEM and XRD data for Mn ₂ O ₃ , [Mn+Sb]O _x and [MnPb+Sb]O _x powder catalysts	23
Figure S24. Comparisons of the XAS data for film and powder [Mn+Sb]O _x and [MnPb+Sb]O _x catalysts ...	24
Figure S25. <i>In situ</i> EXAFS and FT EXAFS data for Mn ₂ O ₃ , [Mn+Sb]O _x and [MnPb+Sb]O _x	25
12 COMPARISONS TO THE LITERATURE	26
Table S3. Activity of the selected noble-metal free acidic OER catalysts.	26

1 | ENERGY DISPERSIVE X-RAY MAPPING

a: $[\text{Mn}+\text{Sb}]\text{O}_x$



b: $[\text{MnPb}+\text{Sb}]\text{O}_x$

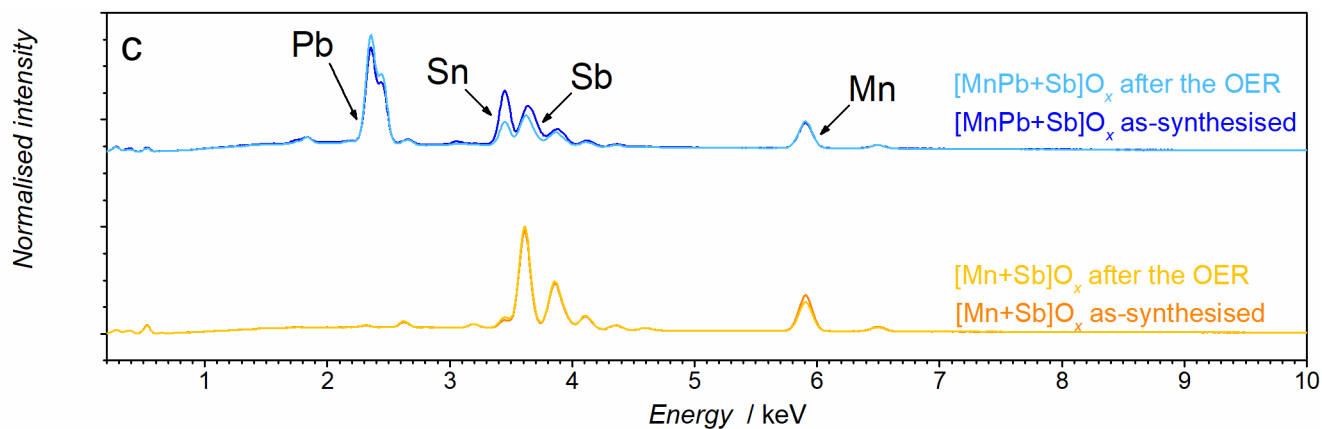
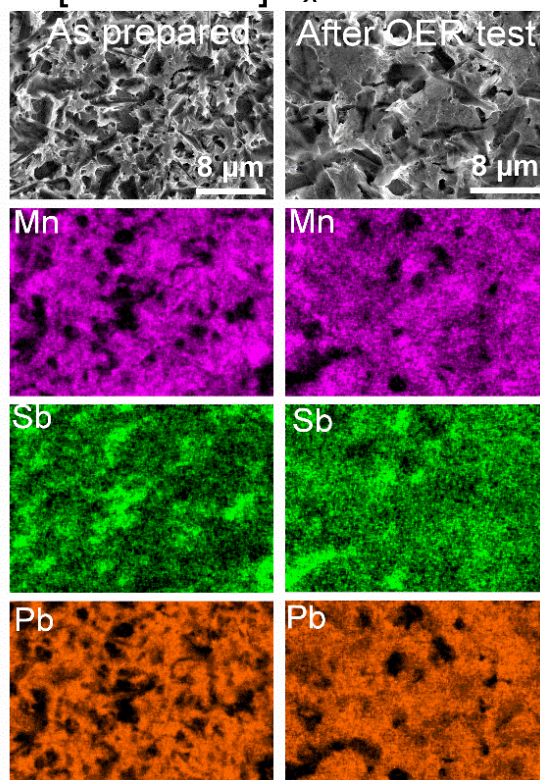


Figure S1. SEM-EDS mapping of the (a) $[\text{Mn}+\text{Sb}]\text{O}_x$ and (b) $[\text{MnPb} + \text{Sb}]\text{O}_x$ before and after OER tests in stirred 0.5 M H_2SO_4 . (c) EDS spectra of the respective samples. The catalysts were tested subsequently for 24 h at 10 mA cm^{-2} , 0.5 h at 2.03 V vs. RHE, and 0.5 h at 1.93 V vs. RHE at ambient temperature.

2 | X-RAY PHOTOELECTRON SPECTROSCOPY

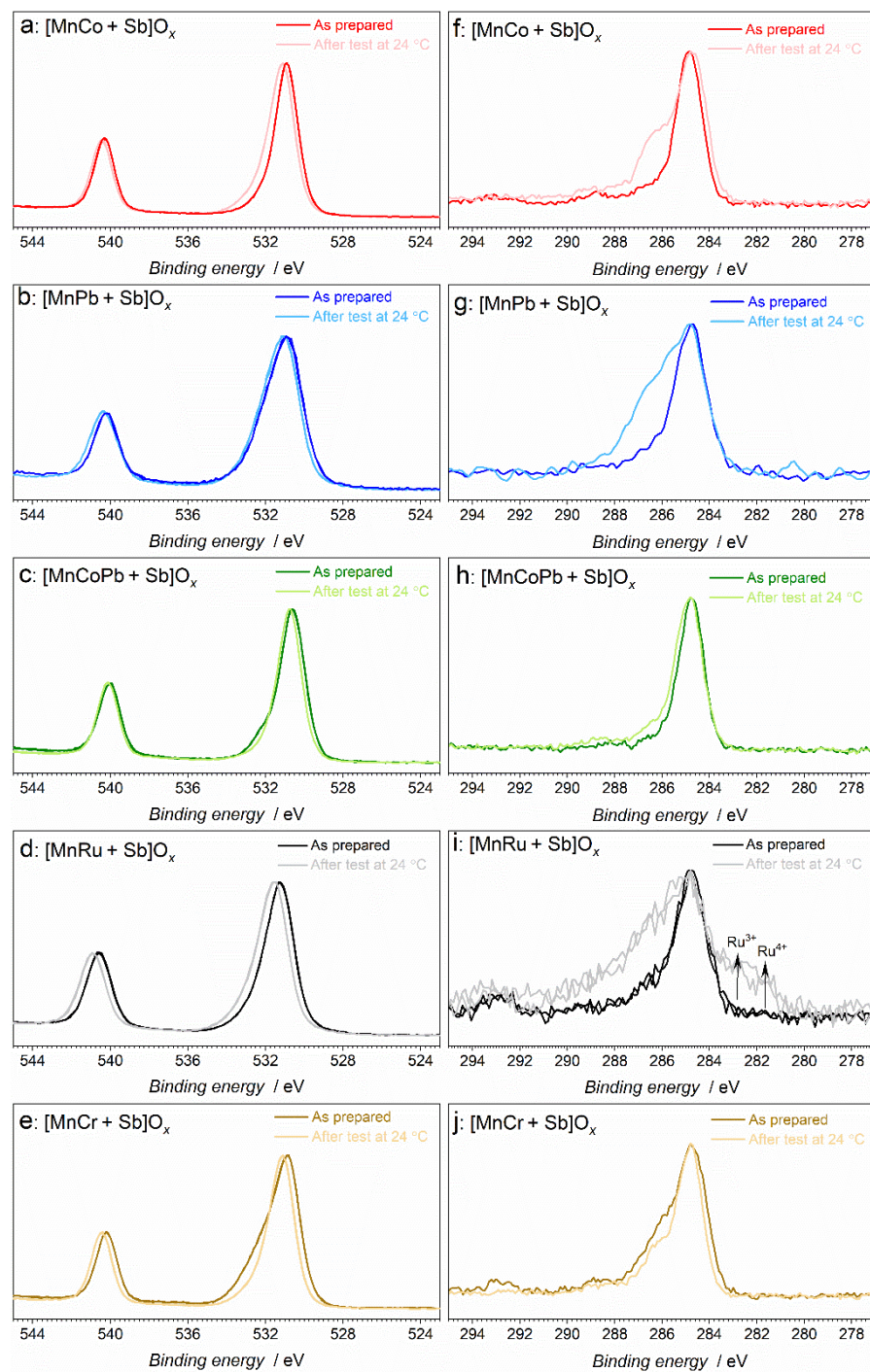


Figure S2. (a-e) Sb 3d + O 1s and (f-j) C 1s (+ Ru 3d) spectra for the (a, f) [MnCo + Sb]O_x, (b, g) [MnPb + Sb]O_x, (c, h) [MnCoPb + Sb]O_x, (d, i) [MnRu + Sb]O_x and (e, j) [MnCr + Sb]O_x catalysts before (vivid traces) and after (pale traces) electrocatalytic OER tests in stirred 0.5 M H₂SO₄. The catalysts were tested subsequently for 24 h at 10 mA cm⁻², 0.5 h at 2.03 V vs. RHE, and 0.5 h at 1.93 V vs. RHE at ambient temperature.

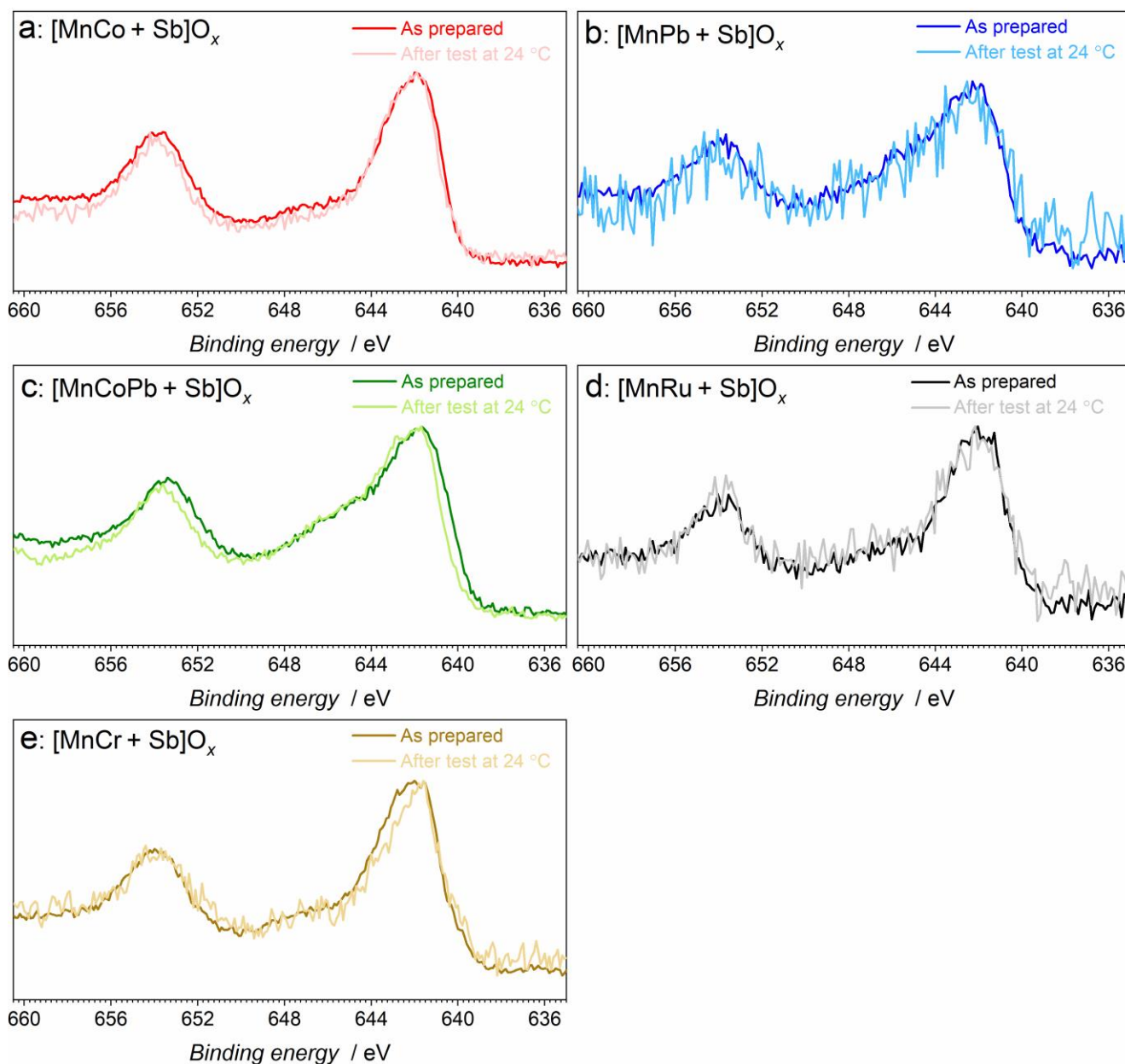


Figure S3. Mn 2p spectra for (a) $[\text{MnCo}+\text{Sb}]\text{O}_x$, (b) $[\text{MnPb}+\text{Sb}]\text{O}_x$, (c) $[\text{MnCoPb}+\text{Sb}]\text{O}_x$, (d) $[\text{MnRu}+\text{Sb}]\text{O}_x$ and (e) $[\text{MnCr}+\text{Sb}]\text{O}_x$ before (vivid traces) and after (pale traces) electrocatalytic OER tests in stirred 0.5 M H_2SO_4 . The catalysts were tested subsequently for 24 h at 10 mA cm^{-2} , 0.5 h at 2.03 V vs. RHE, and 0.5 h at 1.93 V vs. RHE at ambient temperature.

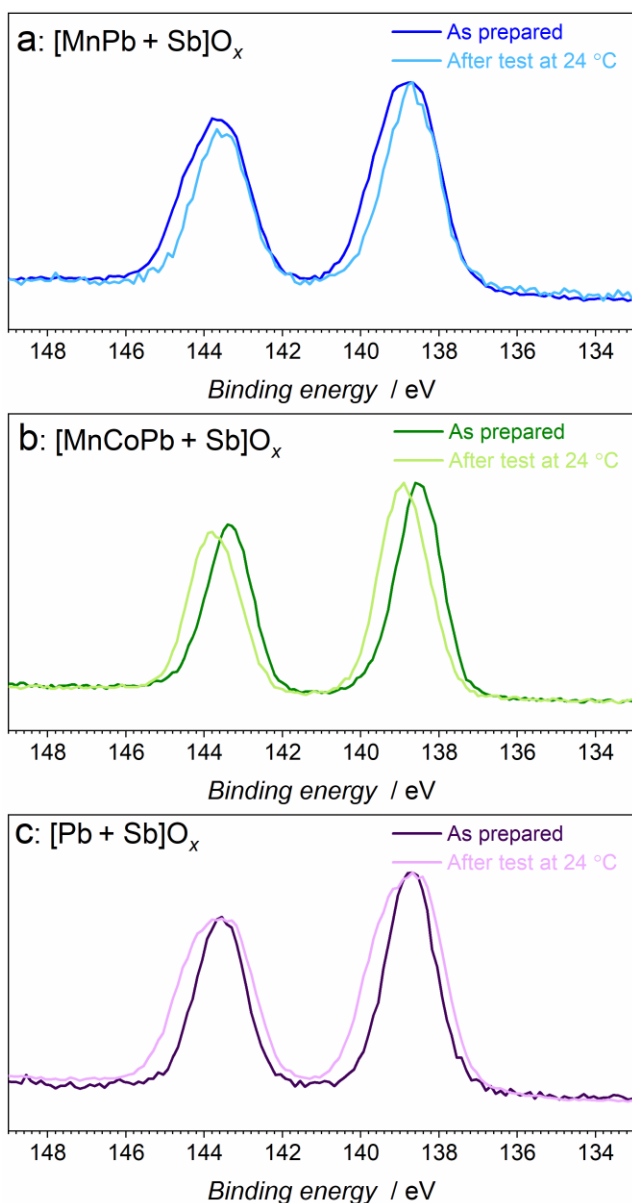


Figure S4. Pb 4f spectra for (a) [MnPb+Sb]O_x, (b) [MnCoPb+Sb]O_x and (c) [Pb+Sb]O_x before (vivid traces) and after (pale traces) electrocatalytic OER tests in stirred 0.5 M H₂SO₄. The catalysts were tested subsequently for 24 h at 10 mA cm⁻², 0.5 h at 2.03 V vs. RHE, and 0.5 h at 1.93 V vs. RHE at ambient temperature. There were likely at least two component giving rise to signals with slightly different binding energies (within <0.5 eV) contributing to the detected Pb 4f spectra and changing in their ratio to each other before and after tests; however, we could not establish any conclusive trends associated with these observations.

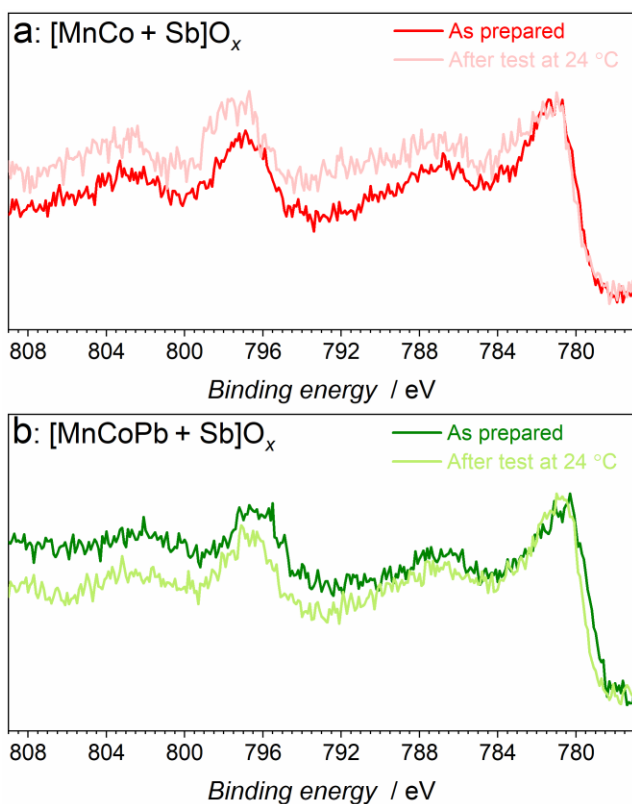


Figure S5. Co 2p spectra for (a) [MnCo+Sb]O_x, and (b) [MnCoPb+Sb]O_x before (vivid traces) and after (pale traces) electrocatalytic OER tests in stirred 0.5 M H₂SO₄. The catalysts were tested subsequently for 24 h at 10 mA cm⁻², 0.5 h at 2.03 V vs. RHE, and 0.5 h at 1.93 V vs. RHE at ambient temperature.

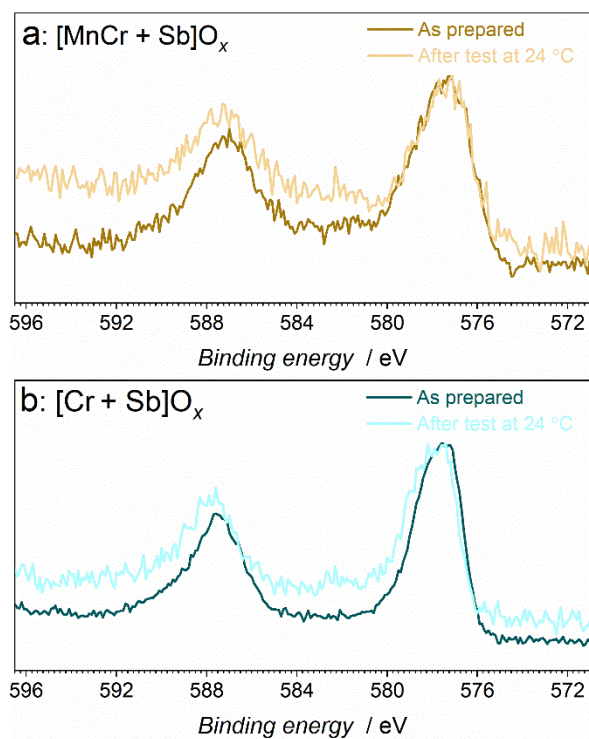


Figure S6. Cr 2p spectra for (a) $[\text{MnCr} + \text{Sb}]\text{O}_x$, and (b) $[\text{Cr} + \text{Sb}]\text{O}_x$ before (vivid traces) and after (pale traces) electrocatalytic OER tests in stirred 0.5 M H_2SO_4 . The catalysts were tested subsequently for 24 h at 10 mA cm^{-2} , 0.5 h at 2.03 V vs. RHE, and 0.5 h at 1.93 V vs. RHE at ambient temperature.

3 | CHANGES IN THE COMPOSITION OF CATALYSTS DURING THE OER

Table S1. Relative concentration of metals on the catalysts surface^a before and after OER tests^b.

Catalyst	As prepared		Tested at 24 ± 2 °C	
	Mn	M	Mn	M
[Mn+Sb]O _x ^c	23	---	14	---
[MnRu+Sb]O _x	9	n.a. ^d	4	n.a. ^d
[MnCr+Sb]O _x	41	16	48	37
[MnCo+Sb]O _x	29	7	13	7
[MnPb+Sb]O _x	13	34	16	5
[MnPbCo+Sb]O _x	15	6 (Pb) 37 (Co)	25	13 (Pb) 51 (Co)

^a Determined by XPS and normalised to the total amount of metals and antimony present on the surface.

^b Chronopotentiometry at 10 mA cm⁻² for 24 h and subsequent chronoamperometry at 2.03 and 1.93 V vs. RHE for 0.5 h at each potential. ^c As reported in [*J. Mat. Chem. A*, 2021, **9**, 27468]. ^d Determination of the Ru concentration is subject to a very significant uncertainty due to the overlap with C 1s.

Table S2. Corrosion of catalysts (%)^a during the OER in 0.5 M H₂SO₄.^b

Catalyst	Mn	M	Sb
[Mn+Sb]O _x ^d	21	---	17
[MnRu+Sb]O _x	42	0	38
[MnCr+Sb]O _x	25	18	11
[MnCo+Sb]O _x	27	17	16
[MnPb+Sb]O _x	2	14	31

^a Molar ratio of the amounts measured in the electrolyte solutions after OER tests using ICP-OES to the amounts of elements initially deposited onto electrodes. ^b Chronopotentiometry at 10 mA cm⁻² and 24 ± 2 °C for 24 h and subsequent chronoamperometry at 2.03 and 1.93 V vs. RHE for 0.5 h at each potential. ^c Data reported in [*J. Mat. Chem. A*, 2021, **9**, 27468].

4 | EX SITU X-RAY ABSORPTION SPECTROSCOPY

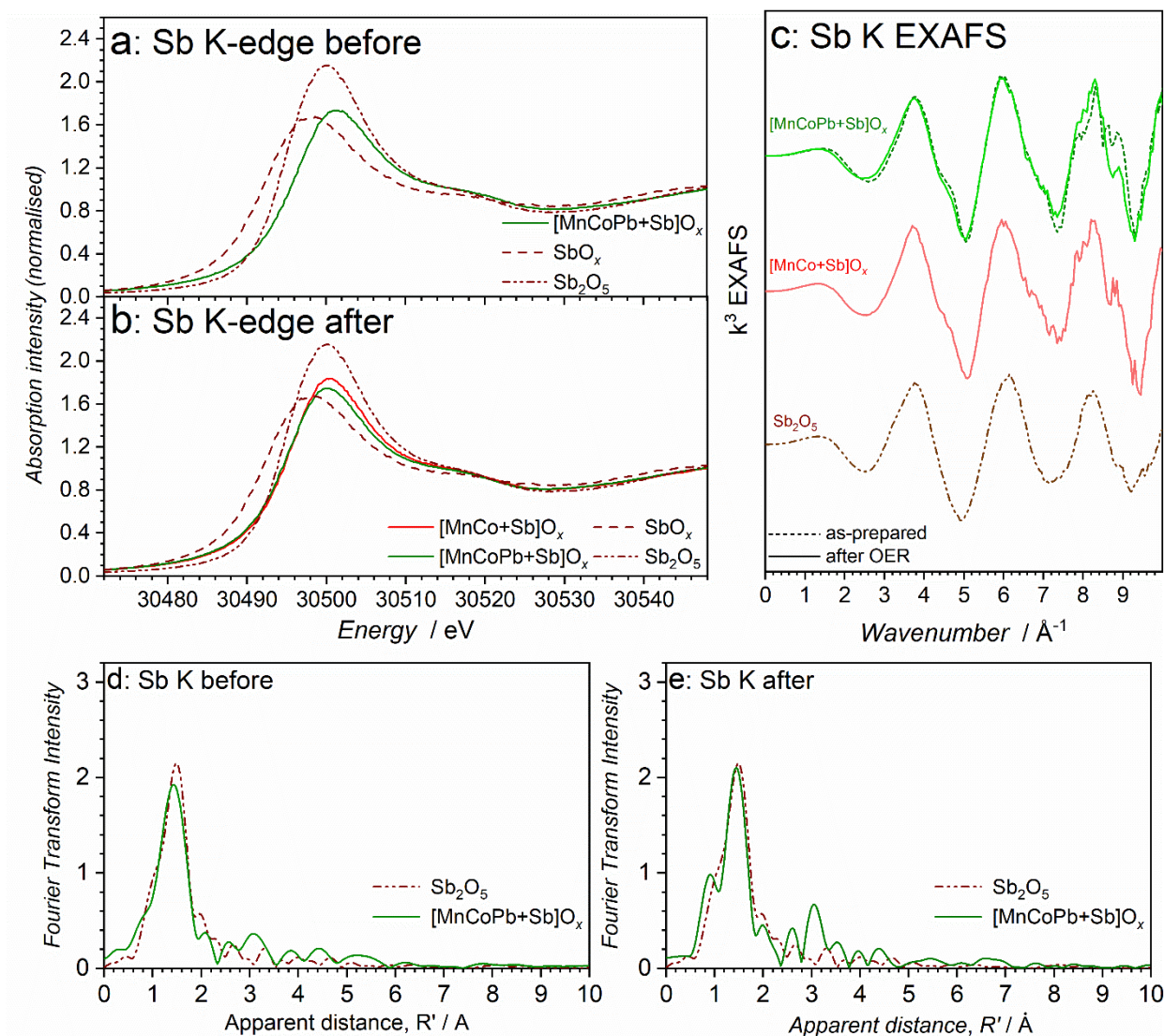


Figure S7. Sb K-edge (a-b) XANES, (c) EXAFS and (d-e) FT-EXAFS data collected for the [MnCo+ Sb]_x (red) and [MnCoPb+ Sb]_x (green) catalysts before and after OER tests (10 mA cm⁻², 24 h, 24 ± 2 °C) compared to relevant reference materials (see figure).

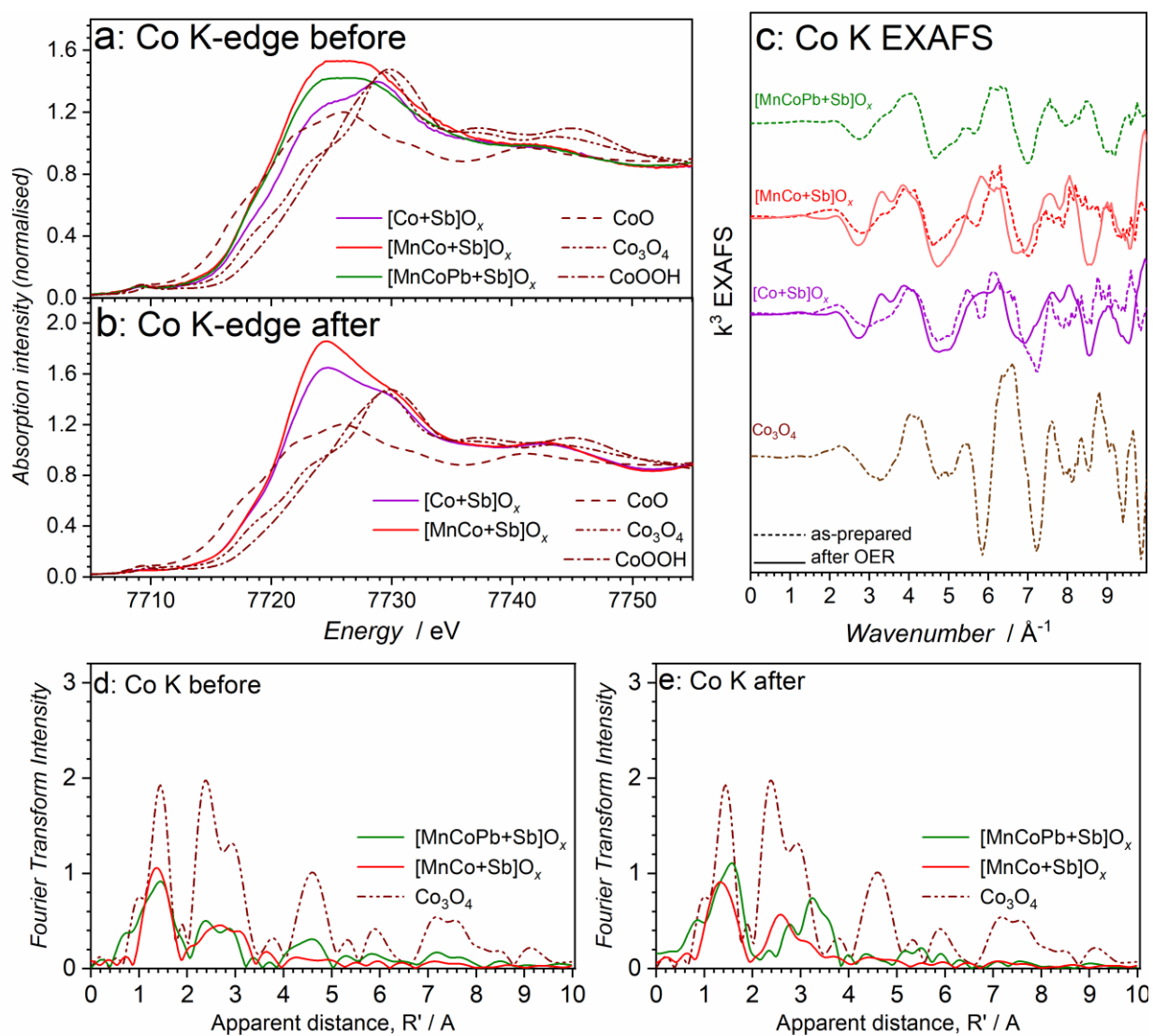


Figure S8. Co K-edge (a-b) XANES, (c) EXAFS and (d-e) FT-EXAFS data collected for the [Co+Sb]O_x (purple), [MnCo+Sb]O_x (red), and [MnCoPb+Sb]O_x (green) catalysts before and after OER tests (10 mA cm⁻², 24 h, 24 ± 2 °C) compared to relevant reference materials (see figure).

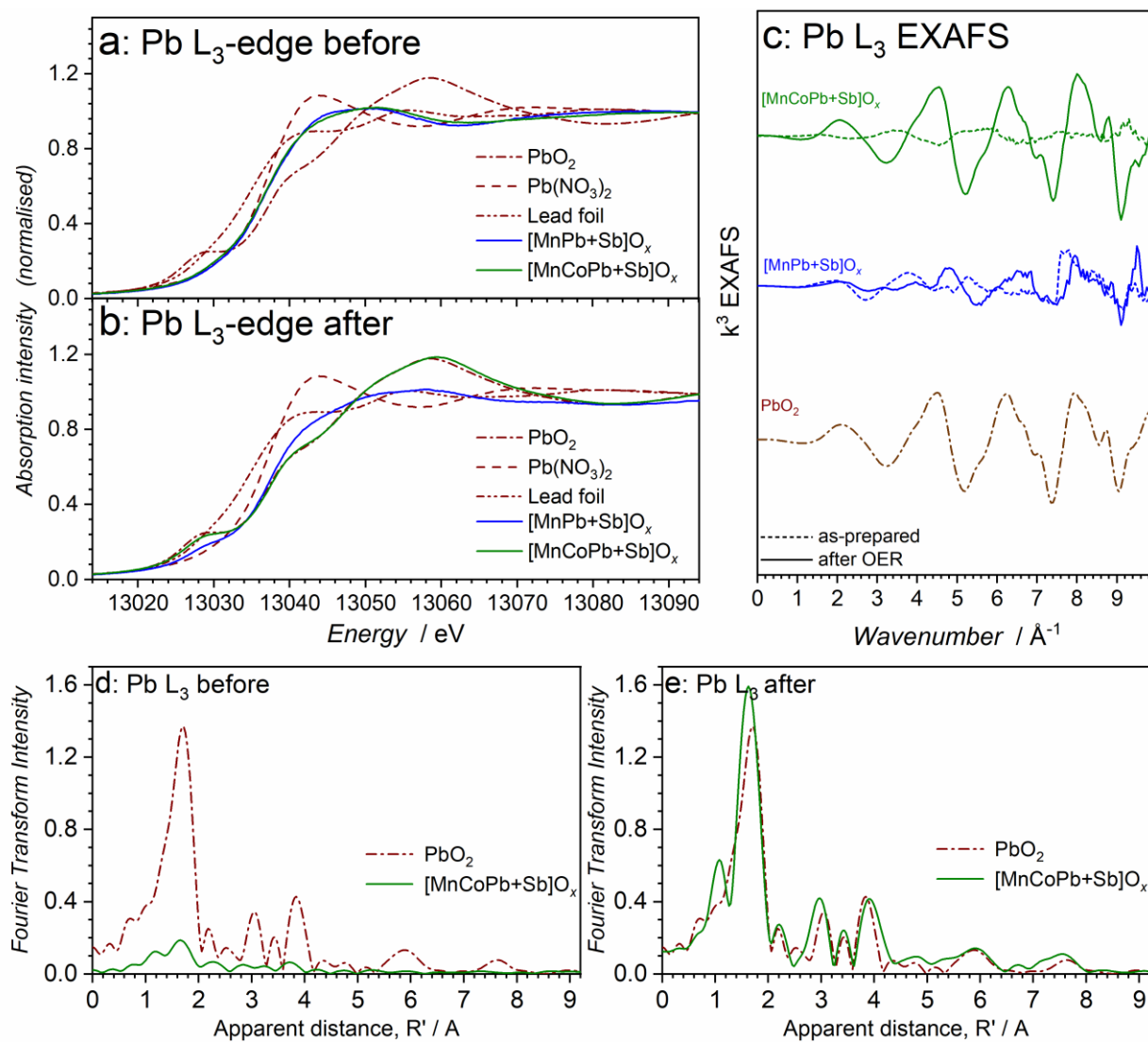


Figure S9. Pb L₃-edge (a-b) XANES, (c) EXAFS and (d-e) FT-EXAFS collected for the [MnPb+Sb]O_x (blue) and [MnCoPb+Sb]O_x (green) catalysts before and after OER tests (10 mA cm⁻², 24 h, 24 ± 2 °C) compared to relevant reference materials (see figure).

5 | OER PERFORMANCE AND REPRODUCIBILITY AT 24 ± 2 °C

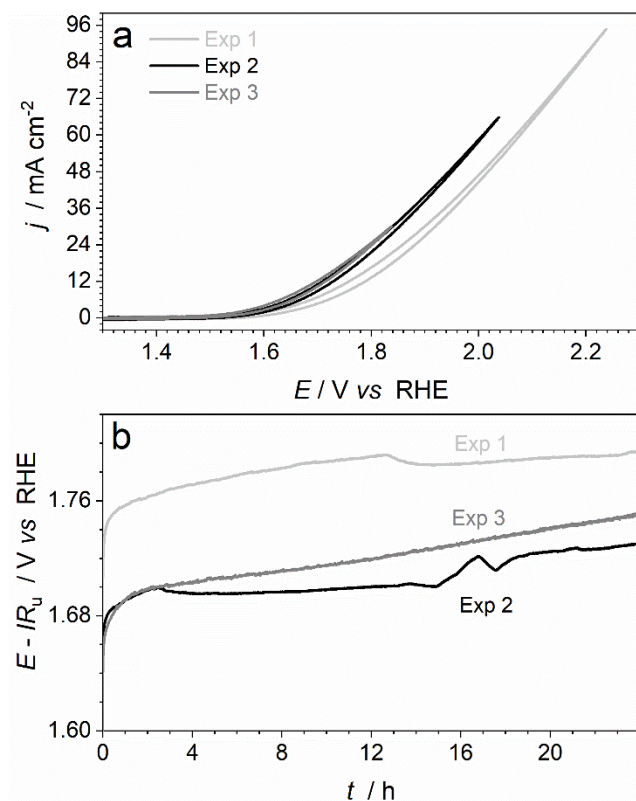


Figure S10. Reproducibility of the electrocatalytic properties of $[\text{MnRu+Sb}]\text{O}_x$ demonstrated for three independent samples tested in stirred 0.5 M H_2SO_4 at 24 ± 2 °C: (a) initial cyclic voltammetry (scan rate 0.020 V s^{-1} ; 3rd scans; potentials are not corrected for ohmic losses; currents are normalised to the geometric surface area), and (b) IR_u -corrected chronopotentiograms at $10 \text{ mA cm}^{-2}_{\text{geom.}}$.

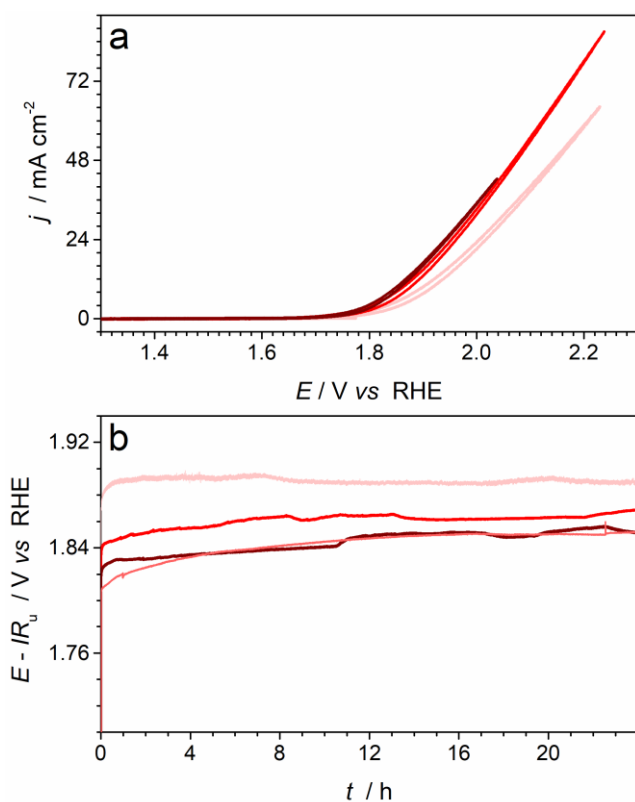


Figure S11. Reproducibility of the electrocatalytic properties of [MnCo+Sb]O_x demonstrated for three independent samples tested in stirred 0.5 M H₂SO₄ at 24 ± 2 °C: (a) initial cyclic voltammetry (scan rate 0.020 V s⁻¹; 3rd scans; potentials are not corrected for ohmic losses; currents are normalised to the geometric surface area), and (b) IR_u -corrected chronopotentiograms at 10 mA cm⁻²_{geom.}. Note that voltammetry was not recorded for one of four independent samples examined.

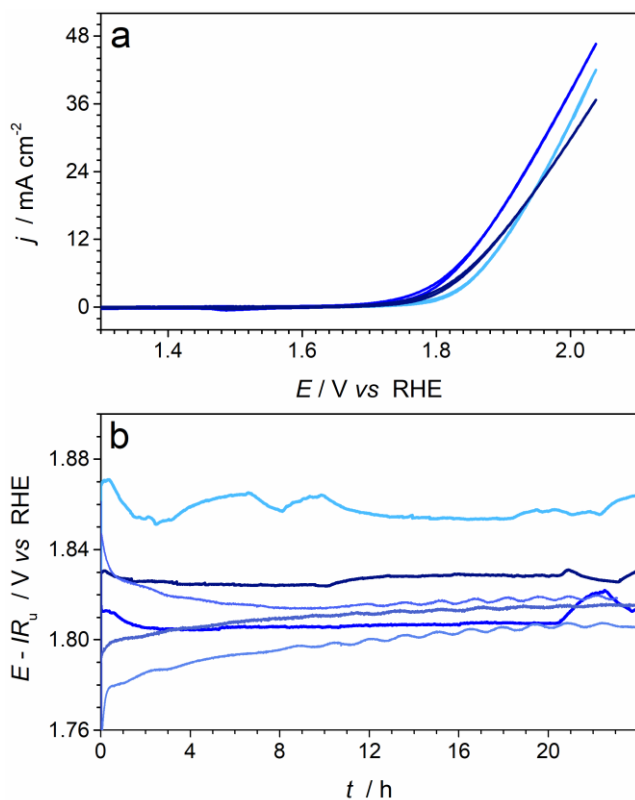


Figure S12. Reproducibility of the electrocatalytic properties of [MnPb+Sb]O_x demonstrated for three independent samples tested in stirred 0.5 M H₂SO₄ at 24 ± 2 °C: (a) initial cyclic voltammetry (scan rate 0.020 V s^{-1} ; 3rd scans; potentials are not corrected for ohmic losses; currents are normalised to the geometric surface area), and (b) IR_u -corrected chronopotentiograms at $10 \text{ mA cm}^{-2}_{\text{geom.}}$. Note that voltammetry was not recorded for three of six independent samples examined.

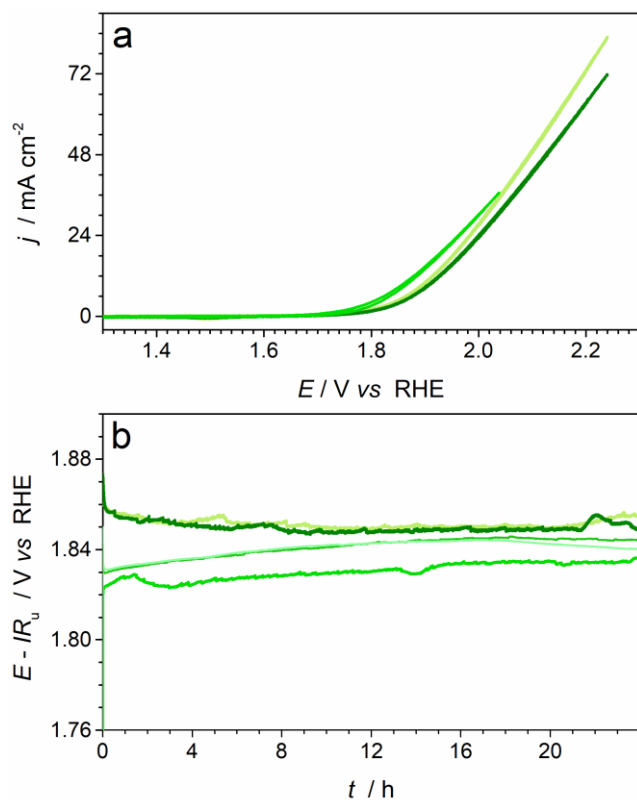


Figure S13. Reproducibility of the electrocatalytic properties of [MnCoPb+Sb]O_x demonstrated for three independent samples tested in stirred 0.5 M H₂SO₄ at 24 ± 2 °C: (a) initial cyclic voltammetry (scan rate 0.020 V s⁻¹; 3rd scans; potentials are not corrected for ohmic losses; currents are normalised to the geometric surface area), and (b) IR_u -corrected chronopotentiograms at 10 mA cm⁻²_{geom.}. Note that voltammetry was not recorded for two of five independent samples examined.

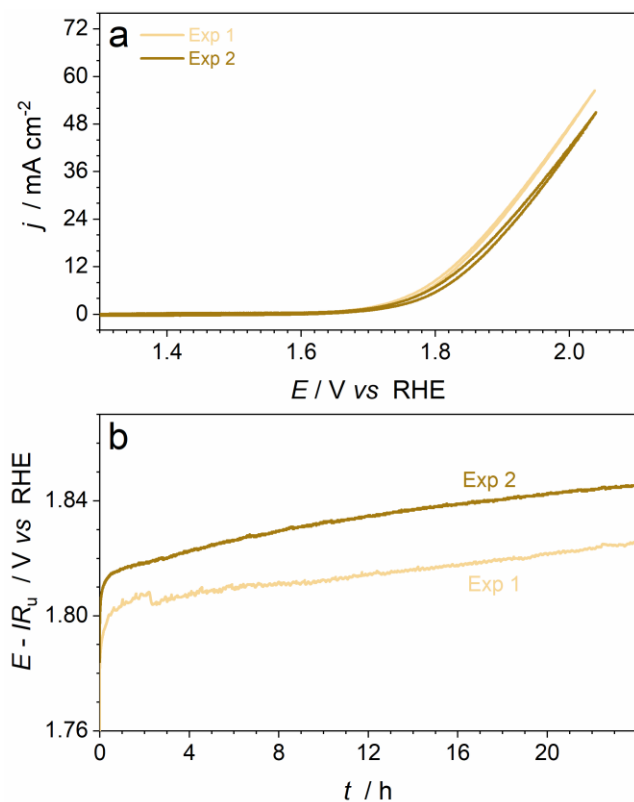


Figure S14. Reproducibility of the electrocatalytic properties of [MnCr+Sb]O_x demonstrated for two independent samples tested in stirred 0.5 M H₂SO₄ at 24 ± 2 °C: (a) initial cyclic voltammetry (scan rate 0.020 V s^{-1} ; 3rd scans; potentials are not corrected for ohmic losses; currents are normalised to the geometric surface area), and (b) IR_u -corrected chronopotentiograms at $10 \text{ mA cm}^{-2}_{\text{geom}}$.

6 | CYCLIC VOLTAMMETRY AT 24 ± 2 °C

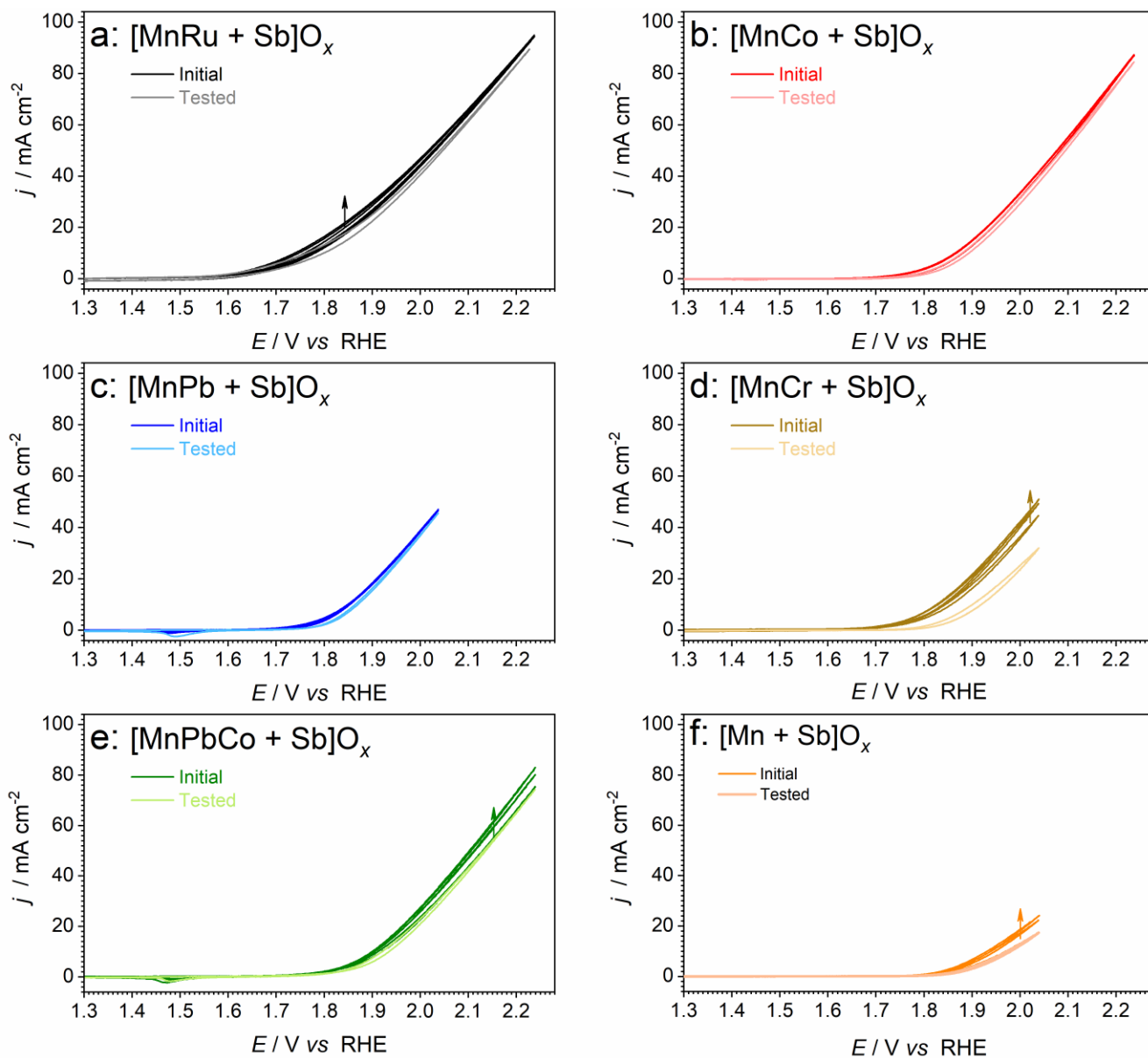


Figure S15. Evolution of cyclic voltammograms (0.020 V s^{-1} ; three consecutive cycles) of (a) [MnRu+Sb] O_x , (b) [MnCo+Sb] O_x , (c) [MnPb+Sb] O_x , (d) [MnCr+Sb] O_x , and (e) [MnPbCo+Sb] O_x in stirred $0.5 \text{ M H}_2\text{SO}_4$ at 24 ± 2 °C. Arrows show the evolution of the current density with cycling. Currents are normalised to the geometric surface area of the electrode; potentials are not corrected for the iR_u -drop.

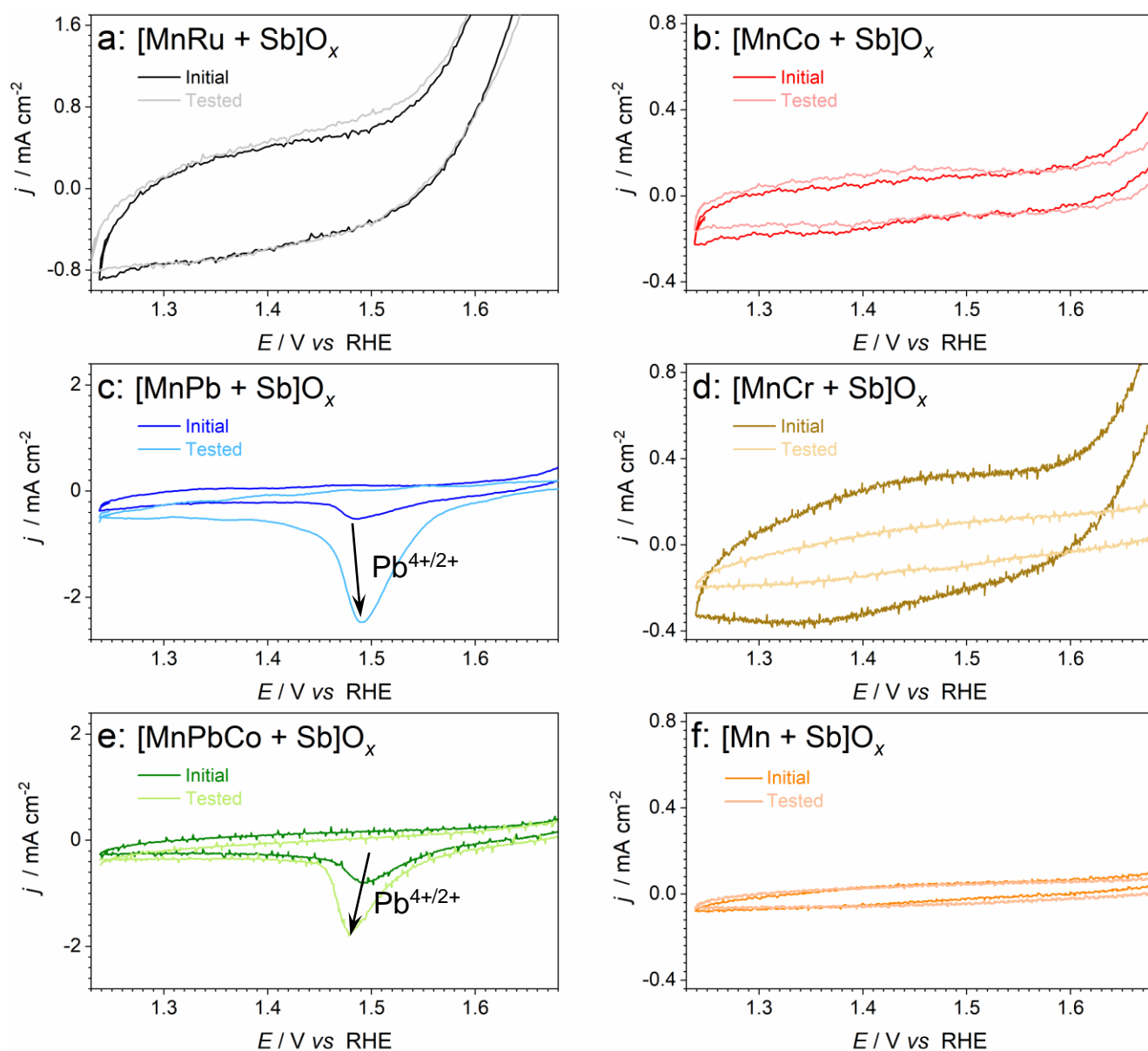


Figure S16. Comparison of the pre-catalytic regions of the quasi-stabilised cyclic voltammograms (0.020 V s^{-1} ; 3rd scans) of (a) [MnRu+Sb]O_x, (b) [MnCo+Sb]O_x, (c) [MnPb+Sb]O_x, (d) [MnCr+Sb]O_x, and (e) [MnPbCo+Sb]O_x, in stirred 0.5 M H₂SO₄ at ambient temperature before (pale traces) and after (vivid traces) 25 h durability tests (24 h at 10 mA cm^{-2} ; 0.5 h at 2.03 V vs. RHE; 0.5 h at 1.93 V vs. RHE) under the same conditions. Arrows in panels (c) and (e) highlight intensification of the $\text{Pb}^{4+/2+}$ reduction process after the OER tests. Currents are normalised to the geometric surface area of the electrode; potentials are not corrected for the IR_u -drop.

7 | OER ACTIVITY OF THE Cr- AND Pb-BASED OXIDES

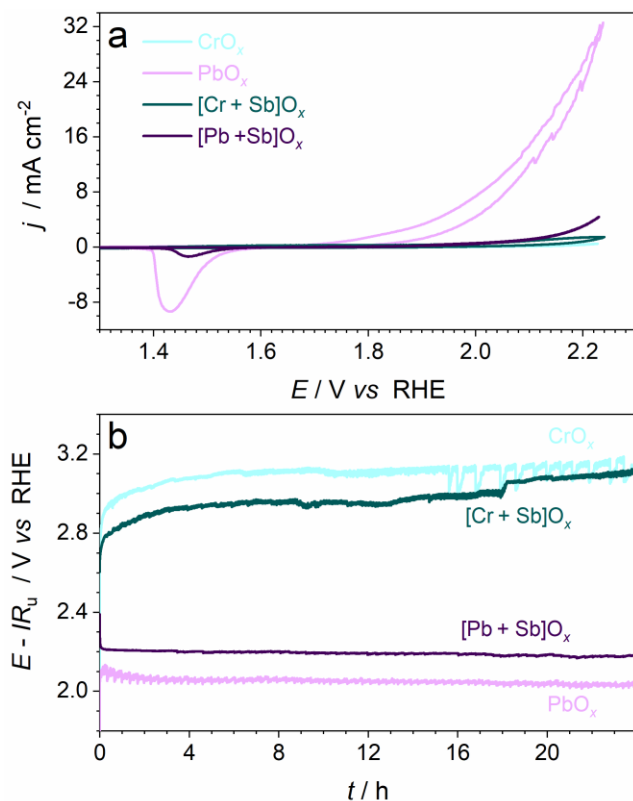


Figure S17. (a) Cyclic voltammetry (0.020 V s^{-1} ; 3rd scans; potentials are not corrected for the IR_u -drop; currents are normalised to the geometric surface area), and (b) IR_u -corrected chronopotentiograms at $10 \text{ mA cm}^{-2}_{\text{geom}}$ recorded for FTO electrodes modified with CrO_y, PbO_y, [Cr+Sb]O_x, and [Pb+Sb]O_x in contact with stirred $0.5 \text{ M H}_2\text{SO}_4$ at $24 \pm 2 \text{ }^\circ\text{C}$.

8 | PERFORMANCE OF [MnCo+Sb]O_x WITH DIFFERENT Mn : Co RATIOS

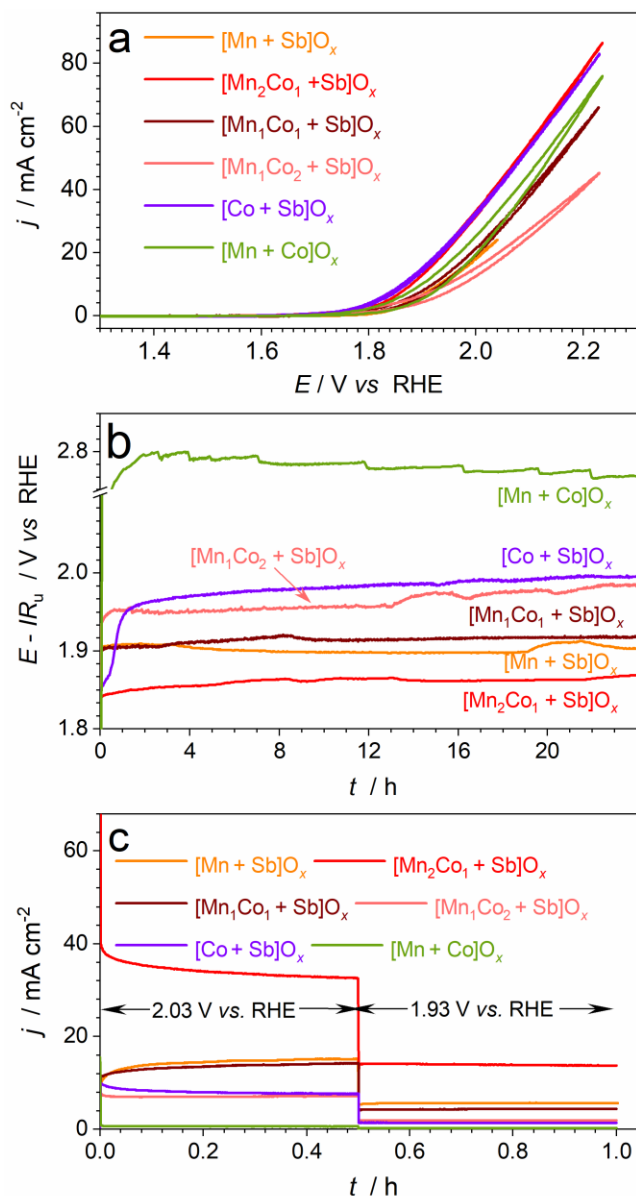


Figure S18. Effect of the Mn : Co initial ratio (see figure) on the performance of the [MnCo+Sb]O_x catalysts in stirred 0.5 M H₂SO₄ at 24 ± 2 °C: (a) cyclic voltammetry (0.020 V s⁻¹; 3rd scans; potentials are not IR_u-corrected; currents are normalised to the geometric surface area), (b) IR_u-corrected chronopotentiograms at 10 mA cm⁻²_{geom.} and (c) chronoamperograms at 2.03 and 1.93 V vs. RHE. Data for the similarly synthesised [Mn+Sb]O_x, [Co+Sb]O_x, and [Mn+Co]O_x are provided for comparison. As reported in [*J. Mater. Chem. A*, 2021, **9**, 27468], the monometallic [Co+Sb]O_x catalyst contains a notable amount of Co₃O₄ admixture enabling reasonable initial performance, which is rapidly lost during first hour of the galvanostatic test, and the resulting performance is ascribed to the actual OER catalytic activity of CoSb₂O₆ – major phase of [Co+Sb]O_x.

9 | OER PERFORMANCE AND REPRODUCIBILITY AT 60 ± 1 °C

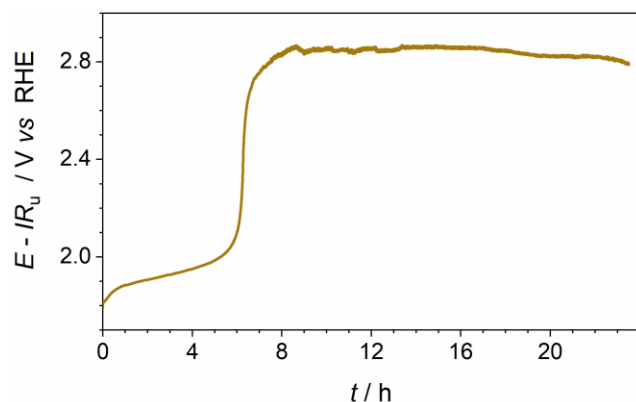


Figure S19. IR_u -corrected chronopotentiogram at $10 \text{ mA cm}^{-2}_{\text{geom.}}$ for $[\text{MnCr+Sb}]\text{O}_x$ tested in stirred $0.5 \text{ M H}_2\text{SO}_4$ at 60 ± 1 °C.

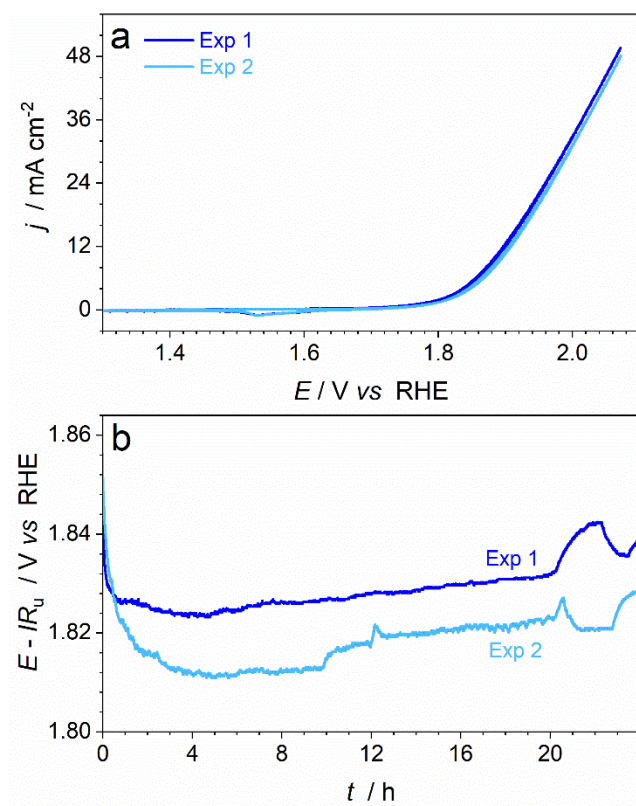


Figure S20. Reproducibility of the electrocatalytic properties of $[\text{MnPb+Sb}]\text{O}_x$ demonstrated for two independent samples tested in stirred $0.5 \text{ M H}_2\text{SO}_4$ at 60 ± 1 °C: (a) initial cyclic voltammetry (0.020 V s^{-1} ; 3rd scans; potentials are not IR_u -corrected; currents are normalised to the geometric surface area), and (b) IR_u -corrected chronopotentiograms at $10 \text{ mA cm}^{-2}_{\text{geom.}}$.

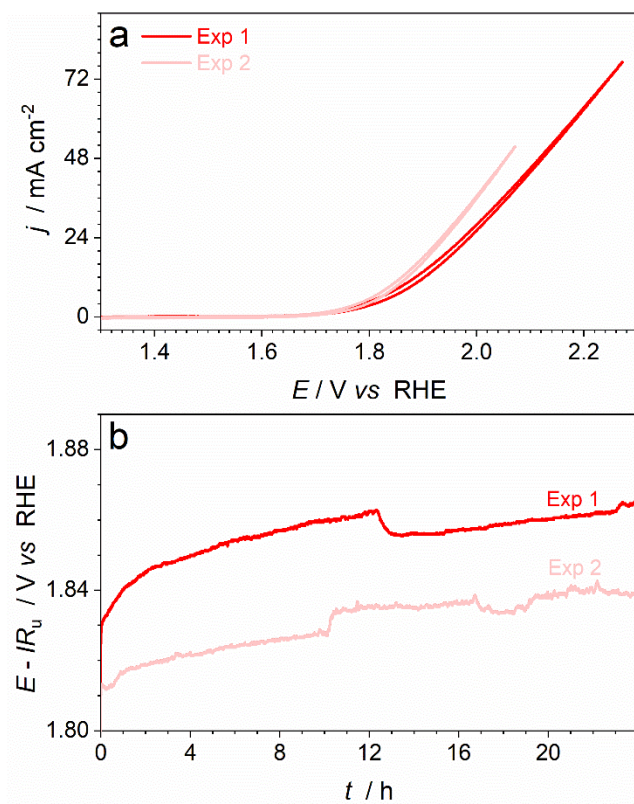


Figure S21. Reproducibility of the electrocatalytic properties of [MnCo+Sb]O_x demonstrated for two independent samples tested in stirred 0.5 M H₂SO₄ at 60 ± 1 °C: (a) initial cyclic voltammetry (0.020 V s⁻¹; 3rd scans; potentials are not IR_u -corrected; currents are normalised to the geometric surface area), and (b) IR_u -corrected chronopotentiograms at 10 mA cm⁻²_{geom.}.

10 | CYCLIC VOLTAMMETRY AT 60 ± 1 °C

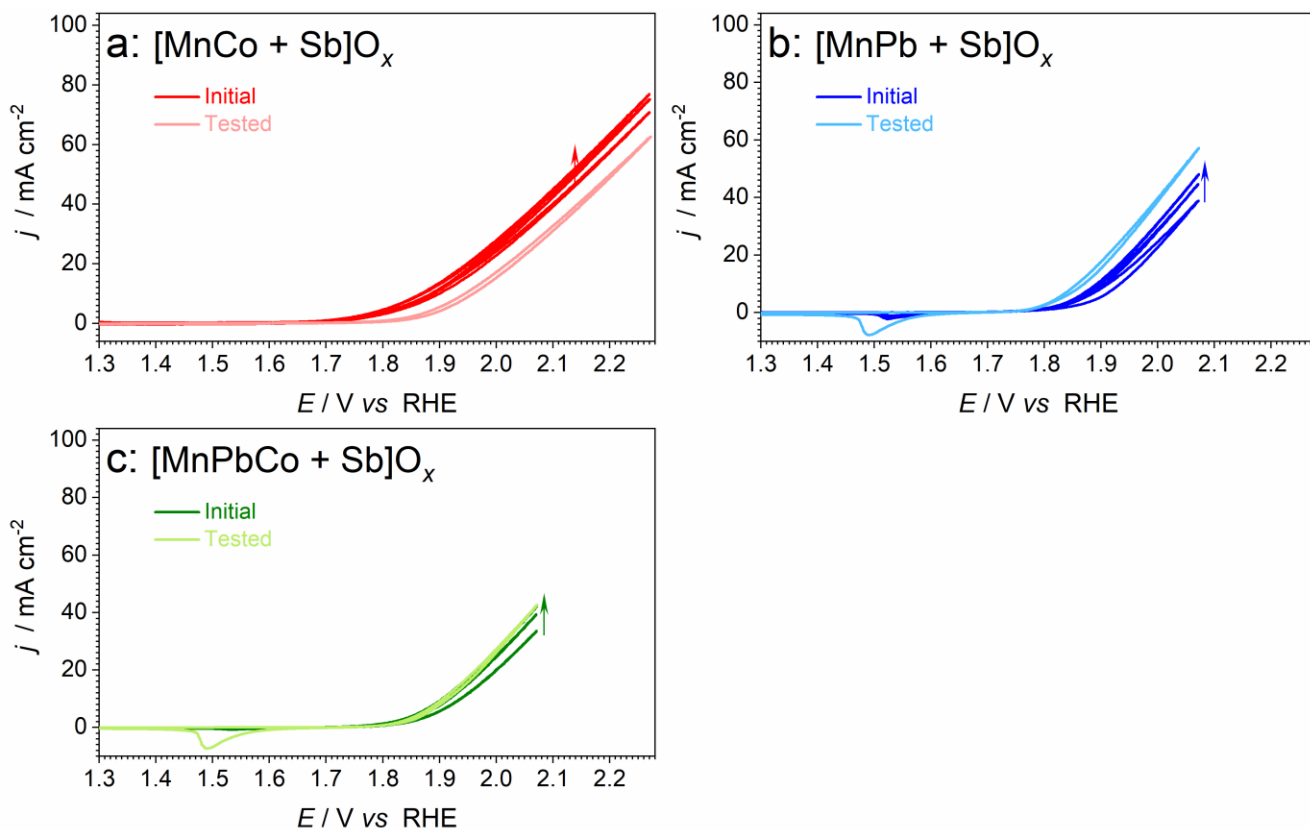


Figure S22. Evolution of cyclic voltammograms (scan rate, $\nu = 0.020 \text{ V s}^{-1}$; three consecutive cycles) of (a) $[\text{MnCo} + \text{Sb}]\text{O}_x$, (b) $[\text{MnPb} + \text{Sb}]\text{O}_x$, and (c) $[\text{MnPbCo} + \text{Sb}]\text{O}_x$ in 0.5 M H_2SO_4 at 60 ± 1 °C. Arrows show the evolution of the current density with cycling. Currents are normalised to the geometric surface area of the electrode; potential values were not corrected for the iR_u -drop.

11 | EXTENDED CHARACTERISATION OF POWDER CATALYSTS

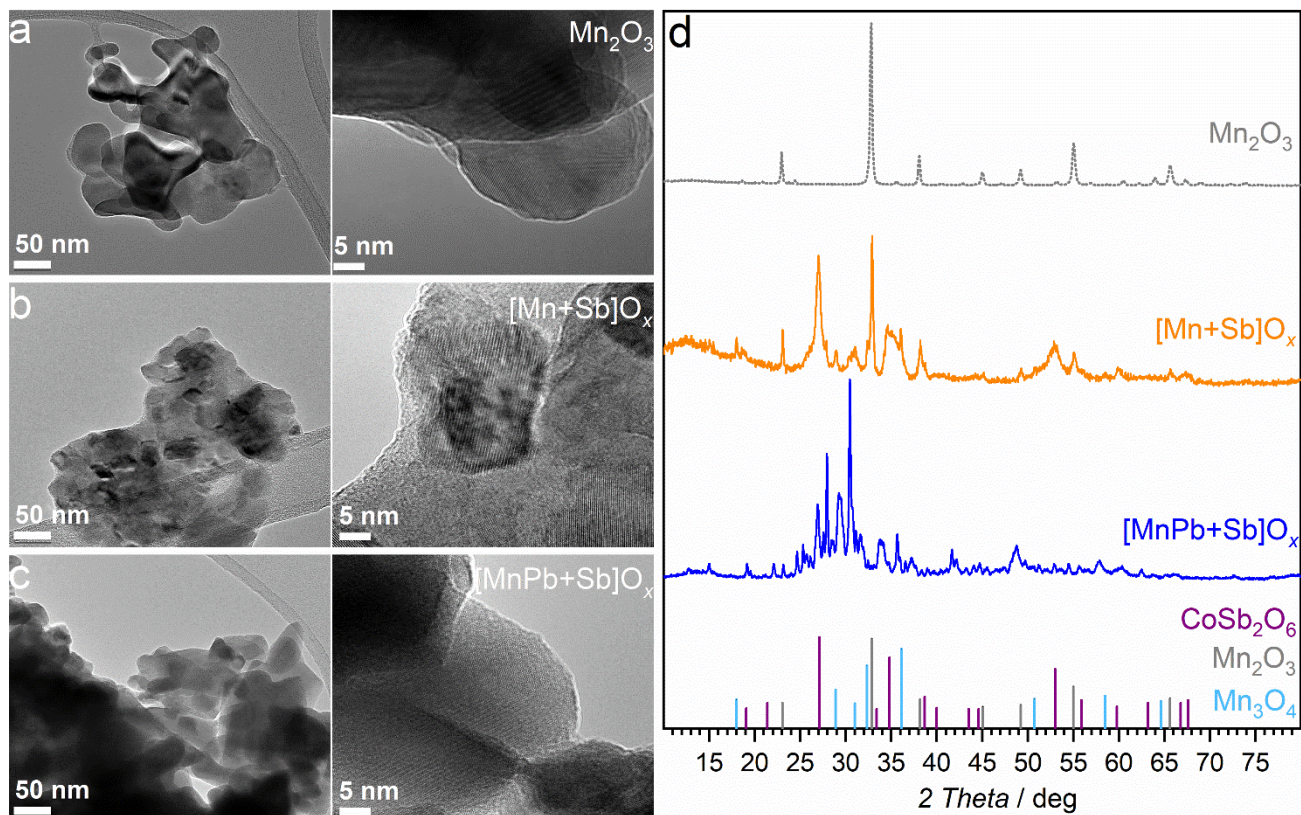


Figure S23. (a-c) Transmission electron micrographs and (d) X-ray diffractograms of the (a, d) Mn₂O₃, (b, d) [Mn+Sb]O_x and (c, b) [MnPb+Sb]O_x powder samples synthesised by the ethylene glycol polyol reduction method. In panel d, vertical lines show tabulated positions and intensities for the Mn₂O₃ (ICDD-00-041-1442), Mn₃O₄ (ICDD-01-075-1560,) and CoSb₂O₆ (ICSD-108964) phases.

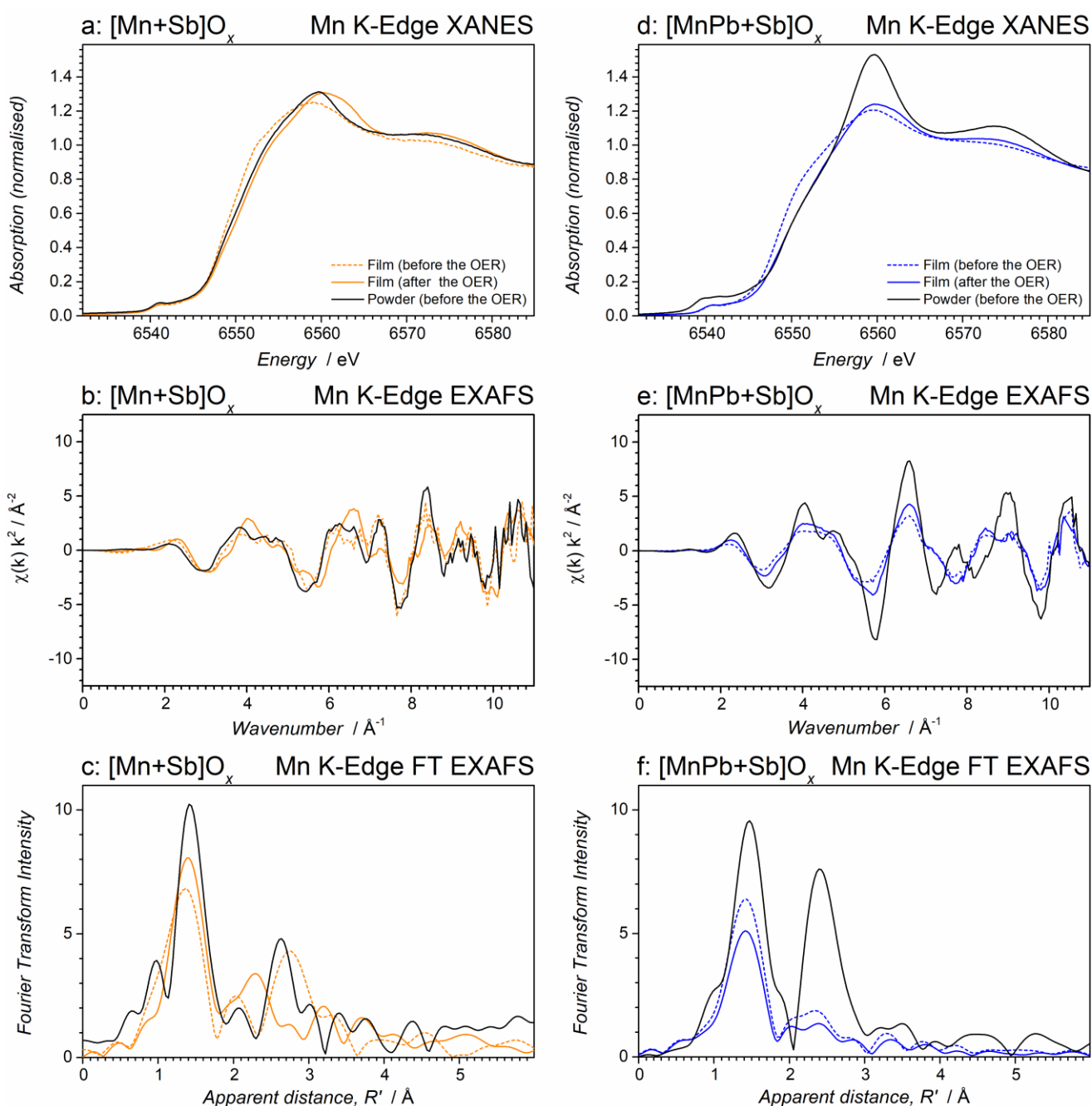


Figure S24. Comparisons of the *ex situ* Mn K-edge XAS data for (a-c) $[\text{Mn}+\text{Sb}]\text{O}_x$ and (d-f) $[\text{MnPb}+\text{Sb}]\text{O}_x$ materials deposited dense films on FTO (orange and blue) and synthesised as powders using an ethylene glycol reduction method (black). For the FTO-supported films, spectra collected before (dashed) and after (solid) the OER tests as those in Figure 3 of the main text are shown. Data are presented as (a, d) XANES, (b, e) EXAFS and (c, f) FT EXAFS spectra.

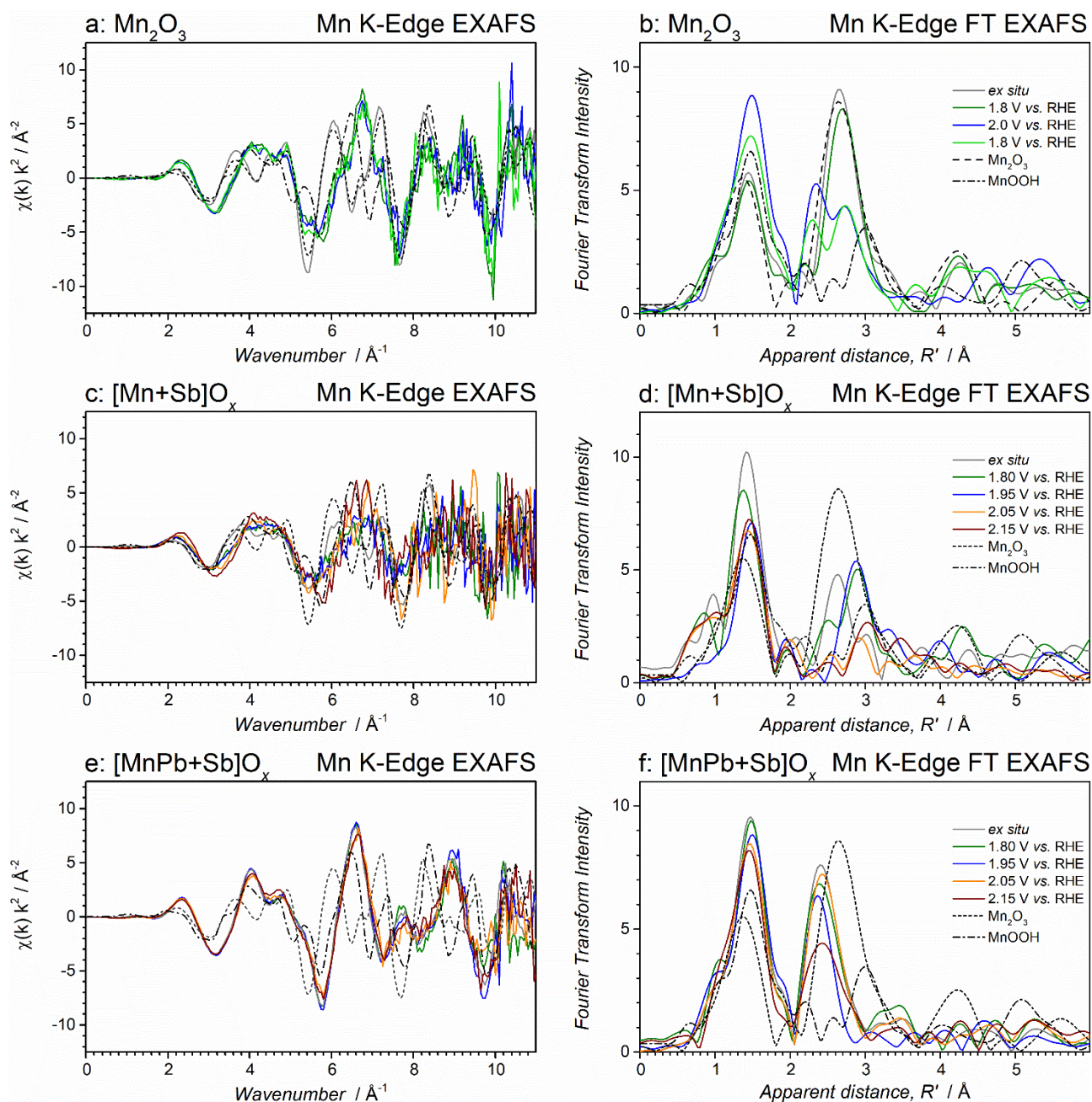


Figure S25. *In situ* Mn K-edge XAS analysis of (a-b) Mn₂O₃, (c-d) [Mn+Sb]O_x and (e-f) [MnPb+Sb]O_x powders collected *ex situ* (grey) and in contact with 0.5 M H₂SO₄ aqueous solutions at 1.80 (green), 1.95 (blue), 2.05 (orange) and 2.15 V vs. RHE (wine) at 23 ± 2 °C. Dashed and dashed-dotted lines show reference data for Mn₂O₃ and MnOOH powders, respectively. For Mn₂O₃, green and light green data were collected at the same potential of 1.8 V vs. RHE before and after analysis at 2.00 V vs. RHE. Data are presented as (a, c, d) EXAFS and (b, d, f) FT EXAFS spectra.

12 | COMPARISONS TO THE LITERATURE

Table S3. Activity of the selected noble-metal free acidic OER catalysts.

Catalyst	Substrate	Electrolyte	E (RHE) / j (geom.) ^a	T / °C	Stability ^b
CoSb ₂ O ₆ ¹	FTO ^c	0.5M H ₂ SO ₄	1.99 V / 10 mA cm ⁻²	ambient	> 24 h
MnSb ₂ O ₆ ¹	FTO ^c	0.5M H ₂ SO ₄	2.17 V / 10 mA cm ⁻²	ambient	> 24 h
Co ₃ O ₄ ²	FTO ^c	0.5 M H ₂ SO ₄	1.8 V / 10 mA cm ⁻²	ambient	< 12 h
Ti/MnO ₂ ³	Au	0.05 M H ₂ SO ₄	1.9 V / 6 mA cm ⁻²	ambient	< 1 h
Ni _x Mn _{1-x} Sb _{1.6} O _y ⁴	ATO ^d	1 M H ₂ SO ₄	1.97 V / 10 mA cm ⁻²	ambient	< 168 h
CoBiSnO _x ⁵	FTO ^c	0.1 M H ₂ SO ₄	1.90 V / 10 mA cm ⁻²	23 ± 2	> 210 h
NiFeP ⁶	Bulk solid	0.05 M H ₂ SO ₄	1.76 V / 10 mA cm ⁻²	ambient	< 30 h
[Mn+Sb]O _x ⁷	FTO ^c	0.5 M H ₂ SO ₄	1.92 V / 10 mA cm ⁻²	23 ± 2	> 25 h
[Mn+Sb]O _x ^{Present work}	FTO ^c	0.5 M H ₂ SO ₄	1.88 V / 10 mA cm ⁻²	60 ± 1	< 10 h
BiO _x ⁸	FTO ^c	0.1 M H ₂ SO ₄	2.00 V / 1 mA cm ⁻²	ambient	> 70 h
Co ₂ MnO ₄ ⁹	FTO ^c	0.1 M H ₂ SO ₄	1.75 V / 100 mA cm ⁻²	ambient	< 200 h
[Ag+Bi]O _x ¹⁰	FTO ^c	0.1 M H ₂ SO ₄	1.93 V / 10 mA cm ⁻²	23 ± 2	> 400 h
			1.81 V / 10 mA cm ⁻²	80 ± 1	> 80 h
[Co-Fe-Pb]O _x ¹¹	Pt-Ti ^e	0.5 M H ₂ SO ₄ + 5 mM Co ²⁺	1.76 V / 10 mA cm ⁻²	80 ± 1	> 160 h
			1.92 V / 100 mA cm ⁻²	80 ± 1	> 29 h ^f
[MnPb+Sb]O _x ^{Present work}	FTO ^c	0.5 M H ₂ SO ₄	1.83 V / 10 mA cm ⁻²	24 ± 2	> 24 h
			1.83 V / 10 mA cm ⁻²	60 ± 1	> 24 h

^a Potentials (E / V vs. RHE) at specified current density (j). ^b Duration of stable operation before degradation commences. ^c Fluorine doped-tin oxide. ^d Antimony doped-tin oxide. ^e Platinised titanium mesh. ^f Note that the performance of [Co-Fe-Pb]O_x is reported incorrectly in Table S1 of Ref¹⁰ due to a misprint.

1. Taylor *et al.* Electrochemical Synthesis and Investigation of Stoichiometric, Phase-Pure CoSb₂O₆ and MnSb₂O₆ Electrodes for the Oxygen Evolution Reaction in Acidic Media. *ACS Appl. Energy Mater.* **2020**, *3*, 5563-5571.
2. Mondschein *et al.* Crystalline Cobalt Oxide Films for Sustained Electrocatalytic Oxygen Evolution under Strongly Acidic Conditions. *Chem. Mater.* **2017**, *29* (3), 950-957.
3. Frydendal *et al.* Toward an Active and Stable Catalyst for Oxygen Evolution in Acidic Media: Ti-Stabilized MnO₂. *Adv. Energy Mater.* **2015**, *5* (22), 1500991.
4. Moreno-Hernandez *et al.* Crystalline nickel manganese antimonate as a stable water-oxidation catalyst in aqueous 1.0 M H₂SO₄. *Energy Environ. Sci.* **2017**, *10* (10), 2103-2108.
5. Du *et al.* Durable Electrooxidation of Acidic Water Catalysed by a Cobalt-Bismuth-based Oxide Composite: An Unexpected Role of the F-doped SnO₂ Substrate. *ChemCatChem* **2022**, *14* (11), e202200013.
6. Hu *et al.* Amorphous Metallic NiFeP: A Conductive Bulk Material Achieving High Activity for Oxygen Evolution Reaction in Both Alkaline and Acidic Media. *Adv. Mater.* **2017**, *29* (32), 1606570.
7. Luke *et al.* Mixed metal-antimony oxide nanocomposites: low pH water oxidation electrocatalysts with outstanding durability at ambient and elevated temperatures. *J. Mater. Chem. A* **2021**, *9* (48), 27468-27484.
8. Thorarinsdottir *et al.* *Chem. Mater.* **2022**, *34* (2), 826-835.
9. Li *et al.* Enhancing the stability of cobalt spinel oxide towards sustainable oxygen evolution in acid. *Nat. Catal.* **2022**, *5* (2), 109-118.
10. Simondson *et al.* Mixed Silver-Bismuth Oxides: A Robust Oxygen Evolution Catalyst Operating at Low pH and Elevated Temperatures. *ACS Catal.* **2022**, *12* (20), 12912-12926.
11. Simondson *et al.* Stable Acidic Water Oxidation with Cobalt-Iron-Lead Oxide Catalyst Operating via a Cobalt-Selective Self-Healing Mechanism. *Angew. Chem. Int. Ed.* **2021**, *60* (29), 15821-15826.